27. Contact Modeling and Manipulation

Imin Kao, Kevin Lynch, Joel W. Burdick

Robotic manipulators use contact forces to grasp and manipulate objects in their environments. Fixtures rely on contacts to immobilize workpieces. Mobile robots and humanoids use wheels or feet to generate the contact forces that allow them to locomote. Modeling of the *contact interface*, therefore, is fundamental to analysis, design, planning, and control of many robotic tasks.

This chapter presents an overview of the modeling of contact interfaces, with a particular focus on their use in manipulation tasks, including graspless or *nonprehensile* manipulation modes such as pushing. Analysis and design of grasps and fixtures also depends on contact modeling, and these are discussed in more detail in Chap. 28. Sections 27.2–27.5 focus on rigid-body models of contact. Section 27.2 describes the kinematic constraints caused by contact, and Sect. 27.3 describes the contact forces that may arise with Coulomb friction. Section 27.4 provides examples of analysis of multicontact manipulation tasks with rigid bodies and Coulomb friction. Section 27.5 extends the analysis to manipulation by pushing. Section 27.6 introduces modeling of contact interfaces, kinematic duality, and pressure distribution. Section 27.7 describes the concept of the friction limit surface and illustrates it with an example demonstrating the construction of a limit surface for a soft contact. Finally, Sect. 27.8 discusses how these more accurate models can be used in fixture analysis and design.

27.1 Overview

A contact model characterizes both the forces that can be transmitted through the contact as well as the allowed relative motions of the contacting bodies. These char-

acteristics are determined by the geometry of the contacting surfaces and the material properties of the parts, which dictate friction and possible contact deformation.

27.1.1 Choosing a Contact Model

The choice of a contact model largely depends upon the application or analysis that must be carried out. When appropriate analytical models are used, one can determine if a manipulation plan or fixture design meets desired functional requirements within the model's limits.

Rigid–Body Models

Many approaches to manipulation, grasp, and fixture analysis are based on rigid-body models. In the rigid-body model, no deformations are allowed at the points or surfaces of contact between two bodies. Instead, contact forces arise from two sources: the constraint of incompressibility and impenetrability between the rigid bodies, and surface frictional forces. Rigid-body models are straightforward to use, lead to computationally efficient planning algorithms, and are compatible with solid-modeling software systems. Rigid-body models are often appropriate for answering qualitative questions such as *will this fixture be able to hold my workpiece*? and for problems involving stiff parts with low to moderate contact forces.

Rigid-body models are not capable of describing the full range of contact phenomena, however; for example, rigid-body models cannot predict the individual contact forces of a multiple-contact fixture (the static indeterminacy problem [27.1, 2]). Furthermore, workpieces held in fixtures experience non-negligible deformations in many high-force manufacturing operations [27.3–6]. These deformations, which crucially impact machining accuracy, cannot be determined from rigid-body models. Also, a rigid-body model augmented with a Coulomb friction model can lead to mechanics problems that have no solution or multiple solutions [27.7–15]. To overcome the limitations inherent in the rigid-body model, one must introduce compliance into the contact model.

Compliant Models

A *compliant* contact deforms under the influence of applied forces. The forces of interaction at the contact are derived from the *compliance* or *stiffness* model. While compliant contact models are typically more complicated, they have several advantages: they overcome the static indeterminacy inherent to rigid-body models and they predict the deformations of grasped or fixtured parts during loading.

A detailed model of the deformations of real materials can be quite complex. Consequently, for analysis we often introduce *lumped-parameter* or *reduced-order* compliance models having a limited number of variables. In this chapter we summarize a reduced-order *quasi-rigid-body* approach to modeling that can model a variety of compliant materials in a way that is consistent with both the solid mechanics literature and conventional robot analysis and planning paradigms.

Finally, three-dimensional finite-element models [27.16–18] or similar ideas [27.19, 20] can be used to analyze workpiece deformations and stresses in fixtures. While accurate, these numerical approaches have some drawbacks, for example, the grasp stiffness matrix can only be found through difficult numerical procedures. Stiffness matrices are often needed to compute quality measures that are the basis for optimal grasping plans or fixturing designs [27.21, 22]. Thus, these numerical approaches are better suited for verifying final fixture designs.

27.1.2 Grasp/Manipulation Analysis

Once a contact model has been chosen, we can use it to analyze tasks involving multiple contacts. If a part is subject to multiple contacts, the kinematic constraints and force freedoms due to the individual contacts must be combined. This combined analysis facilitates manipulation planning – choosing the contact locations, and possibly the motions or forces applied by those contacts, to achieve the desired behavior of the part. A prime example is the grasping or fixturing problem: choosing contact locations, and possibly contact forces, to prevent motion of a part in the face of external disturbances. This well-studied topic is discussed in greater detail in Chap. 28. Other examples include problems of partial constraint, such as pushing a part or inserting a peg into a hole.

27.2 Kinematics of Rigid–Body Contact

Contact kinematics is the study of how two or more parts can move relative to each other while respecting the rigid-body impenetrability constraint. It also classifies motion in contact as either rolling or slipping.

Consider two rigid bodies whose position and orientation (configuration) is given by the local coordinate column vectors q_1 and q_2, respectively. Writing the composite configuration as $q = (q_1^\top, q_2^\top)^\top$, we define

a *distance* function $d(\boldsymbol{q})$ between the parts that is positive when they are separated, zero when they are touching, and negative when they are in penetration. When $d(\boldsymbol{q}) > 0$, there are no constraints on the motions of the parts. When the parts are in contact ($d(\boldsymbol{q}) = 0$), we look at the time derivatives $\dot{d}, \ddot{d}$, etc., to determine if the parts stay in contact or break apart as they follow a trajectory $\boldsymbol{q}(t)$. This can be determined by the following table of possibilities:

d	$\dot{d}$	$\ddot{d}$	$\ldots$	
> 0				no contact,
< 0				infeasible (penetration),
$= 0$	> 0			breaking contact,
$= 0$	< 0			infeasible (penetration),
$= 0$	$= 0$	> 0		breaking contact,
$= 0$	$= 0$	< 0		infeasible (penetration),
etc.				

The contact is maintained only if all time derivatives are zero.

The first two time derivatives are written

$$\dot{d} = \left(\frac{\partial d}{\partial \boldsymbol{q}}\right)^{\top} \dot{\boldsymbol{q}} \,, \tag{27.1}$$

$$\ddot{d} = \dot{\boldsymbol{q}}^{\top} \frac{\partial^2 d}{\partial \boldsymbol{q}^2} \dot{\boldsymbol{q}} + \left(\frac{\partial d}{\partial \boldsymbol{q}}\right)^{\top} \ddot{\boldsymbol{q}} \,. \tag{27.2}$$

The terms $\partial d/\partial \boldsymbol{q}$ and $\partial^2 d/\partial \boldsymbol{q}^2$ carry information about the local contact geometry. The former corresponds to the contact normal, while the latter corresponds to the relative curvature of the parts at the contact.

If contact is maintained, we can classify the contact as slipping or rolling. Analogous to the table above, the contact is rolling if and only if there is zero relative tangential velocity, acceleration, etc., between the contact points on the parts. If the relative tangential velocity is nonzero, the parts are slipping; if the relative velocity is zero but relative tangential acceleration or (higher-order derivatives) is not, slipping is incipient.

In this section we focus on a *first-order* analysis of contact kinematics. A first-order analysis concludes that contact is maintained if $d(\boldsymbol{q}) = 0$ and $\dot{d} = 0$. This local linearization of contact kinematics focuses on the velocity $\dot{\boldsymbol{q}}$ and the contact normal in $\partial d/\partial \boldsymbol{q}$; higher-order spatial derivatives of the contact geometry (curvature, etc.) are not considered. While this is a good starting point, it may occasionally lead to erroneous conclusions. For example, *Rimon* and *Burdick* [27.23–25] showed that a first-order analysis may incorrectly predict mobil-

ity of a part in a fixture when a second-order analysis shows that it is in fact completely constrained.

Analysis of the kinematics of rolling contact of parameterized surfaces can be found in [27.26]; see also [27.27–30].

27.2.1 Contact Constraints

As described in Chap. 1, a rigid body in space has six degrees of freedom, specified by the location of the origin of a coordinate frame P affixed to the part and the orientation of this coordinate frame relative to an inertial frame O fixed in the world. Let ${}^{O}\mathbf{p}_P \in \mathbb{R}^3$ be the position of the part center of mass and ${}^{O}\mathbf{R}_P \in SO(3)$ be the rotation matrix describing the orientation of the part relative to O. The spatial velocity of the part can be written as $\boldsymbol{t} \in \mathbb{R}^6$, sometimes called a *twist*,

$$\boldsymbol{t} = \left(\boldsymbol{\omega}^{\top}, \; \boldsymbol{v}^{\top}\right)^{\top} \,,$$

where $\boldsymbol{\omega} = (\omega_x, \omega_y, \omega_z)^{\top}$ and $\boldsymbol{v} = (v_x, v_y, v_z)^{\top}$ give the angular velocity and linear velocity of P in the world frame O, respectively, such that $\boldsymbol{\omega}$ satisfies

$${}^{O}\dot{\mathbf{R}}_P = \boldsymbol{\omega} \times {}^{O}\mathbf{R}_P$$

and $\boldsymbol{v}$ satisfies

$$\boldsymbol{v} = {}^{O}\dot{\boldsymbol{p}}_P - \boldsymbol{\omega} \times {}^{O}\boldsymbol{p}_P \,.$$

It is worth taking a moment to really understand the spatial velocity of a body. It consists of the body's angular velocity expressed in the world frame O, along with the linear velocity of a point as if it were rigidly attached to the body but currently at the origin of the world frame. This point need not be physically on the body. In other words, $\boldsymbol{v}$ is not simply ${}^{O}\dot{\boldsymbol{p}}_P$. This notation will simplify the following expressions, where all velocities and forces will be expressed in the common world frame O. (Be aware that twists are sometimes defined in a body frame instead.)

A point contact acting on the part provides a unilateral constraint which prevents the part from locally moving against the contact normal. Let $\boldsymbol{x}$ be the location of the contact in O. The linear velocity of the point on the part in contact is

$$\boldsymbol{v}_{\mathrm{C}} = \boldsymbol{v} + \boldsymbol{\omega} \times \boldsymbol{x} \,.$$

(We drop the pre-superscripts O for simplicity; for example, ${}^{O}\boldsymbol{x}$ is written simply as $\boldsymbol{x}$.) Let $\hat{\boldsymbol{u}}$ be the unit vector normal pointing into the part (Fig. 27.1). The first-order condition that the part not move into the unilateral
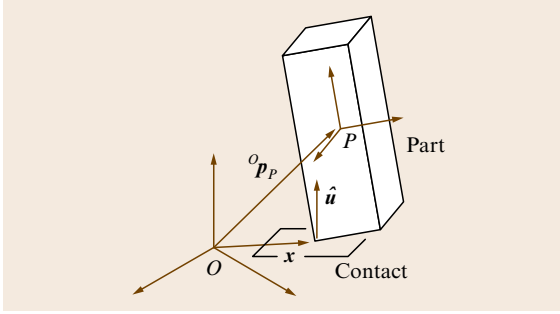
Fig. 27.1 Notation for a part in contact with a manipulator or the environment

constraint can be written

$$v_C^\top \hat{u} = (v + \omega \times x)^\top \hat{u} \geq 0 \ . \qquad (27.3)$$

In other words, the velocity of the part at C cannot have a component in the opposite direction of the contact normal. To write this another way, define a generalized force or *wrench* w consisting of the torque m and force f acting on the part for a unit force along the contact normal:

$$w = (m^\top , f^\top)^\top = [(x \times \hat{u})^\top , \hat{u}^\top]^\top \ .$$

Then (27.3) can be rewritten as

$$t^\top w \geq 0 \ . \qquad (27.4)$$

If the external constraint point is moving with linear velocity v_{ext}, (27.4) changes to

$$t^\top w \geq v_{\text{ext}}^\top \hat{u} \ , \qquad (27.5)$$

which reduces to (27.4) if the constraint is stationary.

Each inequality of the form (27.5) constrains the velocity of the part to a half-space of its six-dimensional velocity space bounded by the hyperplane $t^\top w = v_{\text{ext}}^\top \hat{u}$. Unioning the set of all constraints, we get a convex polyhedral set of feasible part velocities. A constraint is redundant if its half-space constraint does not change the feasible velocity polyhedron. For a given twist t, a constraint is active if

$$t^\top w = v_{\text{ext}}^\top \hat{u} \ ; \qquad (27.6)$$

otherwise the part is breaking contact at that point. In general, the feasible velocity polyhedron for a part can consist of a six-dimensional interior (where no contact constraint is active), five-dimensional hyperfaces, four-dimensional hyperfaces, and so on, down to one-dimensional edges and zero-dimensional points. A part

velocity on an n-dimensional facet of the velocity polyhedron indicates that $6 - n$ independent (nonredundant) constraints are active.

If all of the constraints are stationary ($v_{\text{ext}} = 0$), then each constraining half-plane defined by (27.5) passes through the origin of the velocity space, and the feasible velocity set becomes a cone rooted at the origin. Let w_i be the constraint wrench of stationary contact i. Then the feasible velocity cone is

$$V = \{t \mid t^\top w_i \geq 0 \quad \forall i\} \ .$$

If the w_i span the six-dimensional generalized force space, or, equivalently, the convex hull of the w_i contains the origin in the interior, then the stationary contacts completely constrain the motion of the part, and we have form closure, as discussed in Chap. 28.

In the discussion above, each constraint (27.5) divides the part velocity space into three categories: a hyperplane of velocities that maintain contact, a half-space of velocities that separate the parts, and a half-space of velocities that cause the parts to penetrate. Velocities where the contact is maintained can be further broken down into two categories: velocities where the part slips over the contact constraint, and velocities where the part sticks or rolls on the constraint. In the latter case, the part velocity satisfies the three equations

$$v + \omega \times x = v_{\text{ext}} \ . \qquad (27.7)$$

Now we can give each point contact i a label m_i corresponding to the type of contact, called the contact label: b if the contact is breaking, f if the contact is fixed (including rolling), and s if the contact is slipping, i.e., (27.6) is satisfied but (27.7) is not. The *contact mode* for the entire system can be written as the concatenation of the contact labels at the k contacts, $m_1 m_2 \ldots m_k$.

27.2.2 Collections of Parts

The discussion above can be generalized to find the feasible velocities of multiple parts in contact. If parts i and j make contact at a point x, where $\hat{u}_i$ points into part i and $w_i = [(x \times \hat{u}_i)^\top, \hat{u}_i^\top]^\top$, then their spatial velocities t_i and t_j must satisfy the constraint

$$(t_i - t_j)^\top w_i \geq 0 \qquad (27.8)$$

to avoid penetration. This is a homogeneous half-space constraint in the composite (t_i, t_j) velocity space. In an assembly of multiple parts, each pairwise contact contributes another constraint in the composite part velocity

space, and the result is a polyhedral convex cone of kinematically feasible velocities rooted at the origin of the composite velocity space. The contact mode for the entire assembly is the concatenation of the contact labels at each contact in the assembly.

If there are moving contacts whose motion is prescribed, e.g., robot fingers, the constraints on the motion of the remaining parts will no longer be homogeneous. As a result, the convex polyhedral feasible velocity space is no longer a cone rooted at the origin.

27.2.3 Graphical Planar Methods

When a part is confined to move in the $x–y$-plane, the twist t reduces to $t = (\omega_x, \omega_y, \omega_z, v_x, v_y, v_z)^\top = (0, 0, \omega_z, v_x, v_y, 0)^\top$. The point $(-v_y/\omega_z, v_x/\omega_z)$ is called the center of rotation (CoR) in the projective plane, and we can represent any planar twist by its CoR and rotational velocity ω_z. (Note that the case $\omega_z = 0$ must be treated with care, as it corresponds to a CoR at infinity.) This is sometimes useful for graphical purposes: for a single part constrained by stationary fixtures, at least, we can easily draw the feasible twist cone as CoRs [27.14, 31].

As an example, Fig. 27.2a shows a planar part standing on a table and being contacted by a robot finger. This finger is currently stationary, but we will later set it in motion. The finger defines one constraint on the part's motion and the table defines two more. (Note that contact points in the interior of the edge between the part and the table provide redundant kinematic constraints.) The constraint wrenches can be written

$$\boldsymbol{w}_1 = (0, 0, -1, 0, 1, 0)^\top \ ,$$
$$\boldsymbol{w}_2 = (0, 0, 1, 0, 1, 0)^\top \ ,$$
$$\boldsymbol{w}_3 = (0, 0, 1, -1, 0, 0)^\top \ .$$

For a stationary finger, the kinematic constraints yield the feasible twist cone shown in Fig. 27.2b. This region can also be easily visualized in the plane by using the following method: at each contact, draw the contact normal line. Label all points on the normal $\pm$, points to the left of the inward normal $+$, and points to the right $-$. For each contact constraint, all the points labeled $+$ can serve as CoRs with positive angular velocity, and all the points labeled $-$ can serve as CoRs with negative angular velocity, without violating the contact constraint. After doing this for all the contact normals, keep only the CoRs that are consistently labeled. These CoRs are a planar representation of the feasible twist cone (Fig. 27.2c).
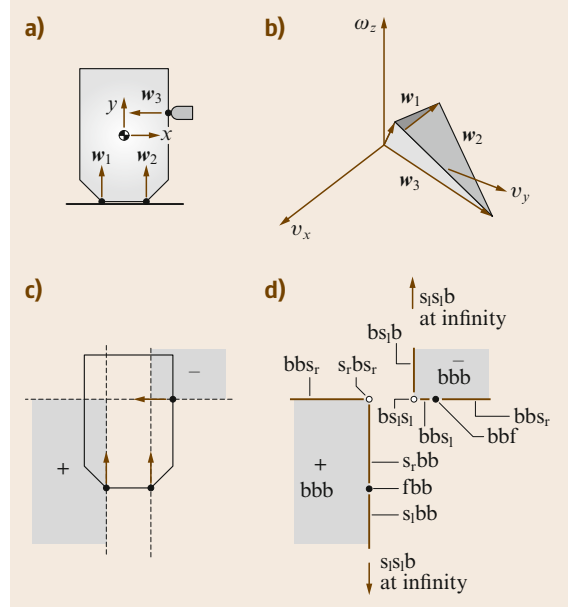
Fig. 27.2 (a) A part resting on a table and the three contact constraints. **(b)** The twist cone satisfying the contact constraints. The contact normals are shown with their associated constraint planes. **(c)** The equivalent representation as CoRs, shown in *grey*. Note that the lines that extend off to the *left* and to the *bottom wrap around* at infinity and come back in from the *right* and the *top*, respectively, so this COR region should be interpreted as a single connected convex region, equivalent to the twist cone representation in **(b)**. **(d)** The contact modes assigned to each feasible motion. The zero velocity contact mode is fff

We can refine this method by assigning contact modes to each feasible CoR. For each contact normal, label the CoR at the contact point f for fixed, other CoRs on the normal line s for slipping, and all other CoRs b for breaking contact. The concatenation of these labels gives the part's contact mode for a particular part motion. In the planar case, the label s on the contact normal line can be further refined into s_r or s_l, indicating whether the part is slipping right or left relative to the constraint. An s CoR labeled $+$ above the contact (in the direction of the contact normal) or $-$ below the contact should be relabeled s_r, and an s CoR labeled $-$ above the contact or $+$ below should be relabeled s_l (Fig. 27.2d).

This method can be used readily to determine if the part is in form closure. If there is no CoR labeled consistently, then the feasible velocity cone consists of only

the zero velocity point, and the part is immobilized by the stationary contacts. This method also makes it clear that at least four contacts are necessary to immobilize the part by the first-order analysis (see also Chap. 28). This is a weakness of the first-order analysis – curvature effects can be used to immobilize a part with three

or even two contacts [27.24]. This weakness can also be seen in Fig. 27.2d. A pure rotation about the CoR labeled $\{+, s_r b s_r\}$ is actually not feasible, but it would be if the part had a small radius of curvature at the contact with the finger. The first-order analysis ignores this curvature.

27.3 Forces and Friction

A commonly used model of friction in robotic manipulation is Coulombs law [27.32]. This experimental law states that the friction force magnitude f_t in the tangent plane at the contact interface is related to the normal force magnitude f_n by $f_t \leq \mu f_n$, where μ is called the friction coefficient. If the contact is sliding, then $f_t = \mu f_n$, and the friction force opposes the direction of motion. The friction force is independent of the speed of sliding.

Often two friction coefficients are defined, a static friction coefficient μ_s and a kinetic (or sliding) friction coefficient μ_k, where $\mu_s \geq \mu_k$. This implies that a larger friction force is available to resist initial motion, but once motion has begun, the resisting force decreases. Many other friction models have been developed with

different functional dependencies on factors such as the speed of sliding and the duration of static contact before sliding. All of these are aggregate models of complex microscopic behavior. For simplicity, we will assume the simplest Coulomb friction model with a single friction coefficient μ. This model is reasonable for hard, dry materials. The friction coefficient depends on the two materials in contact, and typically ranges from 0.1 to 1.

Figure 27.3a shows that this friction law can be interpreted in terms of a *friction cone*. The set of all forces that can be applied to the disk by the supporting line is constrained to be inside this cone. Correspondingly, any force the disk applies to the support is inside the negative of the cone. The half-angle of the cone is $\beta = \tan^{-1} \mu$, as shown in Fig. 27.4. If the disk slips to the left on the support, the force the support applies to it acts on the right edge of the friction cone, with a magnitude determined by the normal force.

If we choose a coordinate frame, the force f applied to the disk by the support can be expressed as a wrench
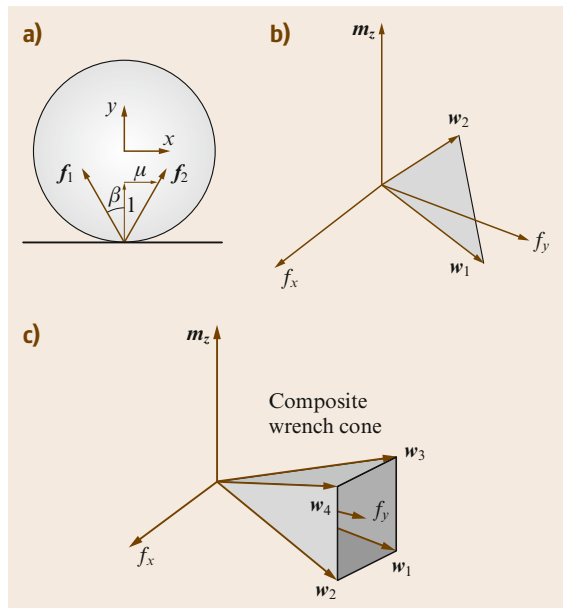
Fig. 27.3 (a) A planar friction cone. **(b)** The corresponding wrench cone. **(c)** An example composite wrench cone resulting from two frictional contacts
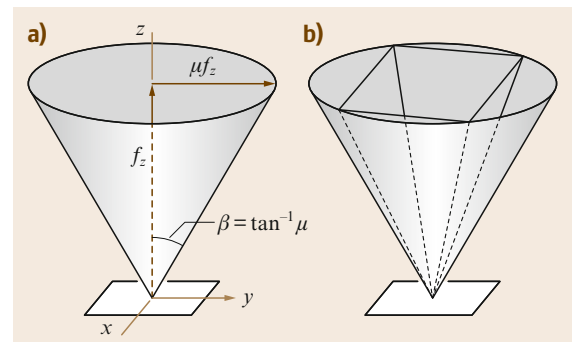
Fig. 27.4 (a) A spatial friction cone. The half-angle of the cone is $\beta = \tan^{-1} \mu$. **(b)** An inscribed pyramidal approximation to the friction cone. A more accurate inscribed pyramidal approximation can be used by increasing the number of faces of the pyramid. Depending on the application, a circumscribed pyramid could be used instead of an inscribed pyramid

$w = [(x \times f)^\top, f^\top]^\top$, where x is the contact location. Thus the friction cone turns into a wrench cone, as shown in Fig. 27.3b. The two edges of the planar friction cone give two half-lines in the wrench space, and the wrenches that can be transmitted to the part through the contact are all nonnegative linear combinations of basis vectors along these edges. If w_1 and w_2 are basis vectors for these wrench cone edges, we write the wrench cone as

$$WC = \{k_1 w_1 + k_2 w_2 \mid k_1, k_2 \geq 0\} .$$

If there are multiple contacts acting on a part, then the total set of wrenches that can be transmitted to the part through the contacts is the nonnegative linear combination of all the individual wrench cones WC_i,

$$WC = \mathrm{pos}(\{WC_i\})$$
$$= \left\{ \sum_i k_i w_i \mid w_i \in WC_i, k_i \geq 0 \right\} .$$

This composite wrench cone is a convex polyhedral cone rooted at the origin. An example composite wrench cone arising from two planar frictional contacts is shown in Fig. 27.3c. If the composite wrench cone is the entire wrench space, then the contacts can provide a force closure grasp (Chap. 28).

In the spatial case, the friction cone is a circular cone, defined by

$$\sqrt{f_x^2 + f_y^2} \leq \mu f_z , \ f_z \geq 0 \tag{27.9}$$

when the contact normal is in the $+z$-direction (Fig. 27.4). The resulting wrench cone, and composite wrench cone $\mathrm{pos}(\{WC_i\})$ for multiple contacts, is a convex cone rooted at the origin, but it is not polyhedral. For computational purposes, it is common to approximate circular friction cones as pyramidal cones, as shown in Fig. 27.4. Then individual and composite wrench cones become polyhedral convex cones in the six-dimensional wrench space.

If a contact or set of contacts acting on a part is ideally force controlled, the wrench w_{ext} specified by the controller must lie within the composite wrench cone corresponding to those contacts. Because these force-controlled contacts choose a subset of wrenches (possibly a single wrench) from this wrench cone, the total composite wrench cone that can act on the part (including other non-force-controlled contacts) may no longer be a homogeneous cone rooted at the origin. This is roughly analogous to the case of velocity-controlled contacts in Sect. 27.2.1, which results in a feasible twist set for the part that is not a cone rooted at the origin. Ideal robot manipulators may be controlled by position

control, force control, hybrid position–force control, or some other scheme. The control method must be compatible with the parts' contacts with each other and the environment to prevent excessive forces [27.33].

27.3.1 Graphical Planar Methods

Just as homogeneous twist cones for planar problems can be represented as convex signed ($+$ or $-$) CoR regions in the plane, homogeneous wrench cones for planar problems can be represented as convex signed regions in the plane. This is called *moment labeling* [27.14, 34]. Given a collection of lines of force in the plane (e.g., the edges of friction cones from a set of point contacts), the set of all nonnegative linear combinations of these can be represented by labeling all the points in the plane with either a '$+$' if all resultants make nonnegative moment about that point, a '$-$' if all make nonpositive moment about that point, a '$\pm$' if all make zero moment about that point, and a blank label if there exist resultants making positive moment and resultants making negative moment about that point.

The idea is best illustrated by an example. In Fig. 27.5a, a single line of force is represented by labeling the points to the left of the line with a $+$ and points to the right of the line with a $-$. Points on the line are labeled $\pm$. In Fig. 27.5b, another line of force is added. Only the points in the plane that are consistently labeled for both lines of force retain their labels; inconsistently labeled points lose their labels. Finally, a third line of force is added in Fig. 27.5c. The result is a single region labeled $+$. A nonnegative combination of the three lines of force can create any line of force in the plane that passes around this region in a counterclockwise sense. This representation is equivalent to a homogeneous convex wrench cone representation.
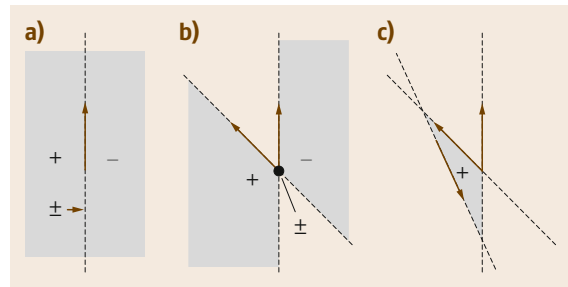
Fig. 27.5 (a) Representing a line of force by moment labels. **(b)** Representing the nonnegative linear combinations of two lines of force by moment labels. **(c)** Nonnegative linear combinations of three lines of force

27.3.2 Duality of Contact Wrenches and Twist Freedoms

Our discussion of kinematic constraints and friction should make it apparent that, for any point contact and contact label, the number of equality constraints on the part's motion caused by that contact is equal to the number of wrench freedoms it provides. For example, a breaking contact b provides zero equality constraints on the part motion and also allows no contact force. A fixed contact f provides three motion constraints (the motion of a point on the part is specified) and three freedoms on the contact force: any wrench in the interior of the contact wrench cone is consistent with the contact mode. Finally, a slipping contact s provides one equality motion constraint (one equation on the part's motion must be satisfied to maintain the contact), and for a given motion satisfying the constraint, the contact wrench has only one freedom, the magnitude of the contact wrench on the edge of the friction cone and opposite the slipping direction. In the planar case, the motion constraints and wrench freedoms for b, s, and f contacts are zero, one, and two, respectively.

At each contact, the force and velocity constraints can be represented by an $n \times 6$ *constraint* or *selection* matrix, $\boldsymbol{H}$ [27.3], at the contact interface. This constraint matrix works like a filter to transmit or deny certain components of motion across the contact interface. By the same token, forces/moments applied across the contact interface are also filtered by the same constraint matrix, $\boldsymbol{H}^\top$, in a dual relationship. Three typical contact models are illustrated below. Contact forces and wrenches are measured in a frame at the contact, with the contact normal in the $+z$-direction.

- The *point contact without friction* model. Only a normal force f_z can be exerted between the contacting bodies:

$$f_z \geq 0, \quad \boldsymbol{w} = \boldsymbol{H}^\top f_z = (0\ 0\ 1\ 0\ 0\ 0)^\top f_z. \quad (27.10)$$

- The *point contact with friction* model includes tangential friction forces, f_x and f_y, in addition to normal force f_z,

$$f_z \geq 0; |f_t| = \sqrt{f_x^2 + f_y^2} \leq \mu f_z,$$

$$\boldsymbol{w} = \boldsymbol{H}^\top \begin{pmatrix} f_x \\ f_y \\ f_z \end{pmatrix} = \begin{pmatrix} 1 & 0 & 0 \\ 0 & 1 & 0 \\ 0 & 0 & 1 \\ 0 & 0 & 0 \\ 0 & 0 & 0 \\ 0 & 0 & 0 \end{pmatrix} \begin{pmatrix} f_x \\ f_y \\ f_z \end{pmatrix}, \quad (27.11)$$

where f_x and f_y are the x- and y-components of the tangential contact force, and f_z is the normal force.

- The *soft finger* contact model with a finite contact patch allows, in addition to the friction and normal forces, a torsional moment with respect to the contact normal [27.35–39]. We have

$$f_z \geq 0;$$

$$\boldsymbol{w} = \boldsymbol{H}^\top \begin{pmatrix} f_x \\ f_y \\ f_z \\ m_z \end{pmatrix} = \begin{pmatrix} 1 & 0 & 0 & 0 \\ 0 & 1 & 0 & 0 \\ 0 & 0 & 1 & 0 \\ 0 & 0 & 0 & 0 \\ 0 & 0 & 0 & 0 \\ 0 & 0 & 0 & 1 \end{pmatrix} \begin{pmatrix} f_x \\ f_y \\ f_z \\ m_z \end{pmatrix}, \quad (27.12)$$

where m_z is the moment with respect to the normal of contact. The finite contact area assumed by the soft contact interface results in the application of a friction moment in addition to the traction forces. If the resultant force on the tangential plane of contact is denoted as $f_t = \sqrt{f_x^2 + f_y^2}$ and the moment with respect to the contact normal is m_z, the following elliptical equation represents the relationship between the force and moment at the onset of sliding:

$$\frac{f_t^2}{a^2} + \frac{m_z^2}{b^2} = 1, \quad (27.13)$$

where $a = \mu f_z$ is the maximum friction force, and $b = (m_z)_{\text{max}}$ is the maximum moment defined in equation (27.32). Further readings on this subject can be found in [27.35–42].

As can be appreciated from the three cases above, the rows of $\boldsymbol{H}$ are the directions along which contact forces are supported. Conversely, relative motions of the two objects are constrained along these same directions: $\boldsymbol{H}\dot{\boldsymbol{q}} = 0$. Thus, the constraint matrix works like a kinematic filter which dictates the components of motions that can be transmitted through the contact interface. The introduction of this matrix makes it easy to model the contact mechanics in analysis using the dual kinematic relationship between force/moment and motion, as described in Table 27.1. For example, the constraint filter matrix in (27.12) describes that all three components of forces and one component of the moment with respect to the normal of contact can be transmitted through the contact interface of a soft finger.

In Chap. 28, when multiple contacts are considered, such $\boldsymbol{H}$ matrices associated with each finger can be con-

Table 27.1 Duality of the kinematics of contact interface. The force/motion relationships for finger and grasped object are dual to each other in the joint space, contact interface, and the Cartesian space of the object. In this table, the notation of θ, x_f, x_p, and x_b are the displacement in the joint space, the Cartesian space at the contact point on the finger, the Cartesian space at the contact point on the object, and the reference frame on the object, respectively, with x_{tr} denoting the transmitted components. The δ prefix denotes infinitesimal changes in the named coordinates. The forces with corresponding subscripts are referenced to the corresponding coordinates as those of the displacement described above

Motion	$\mathbf{J}_\theta$ $\quad \delta\theta \quad = \delta x_f$	$\mathbf{H} \quad \delta x_f = \delta x_{tr} = \mathbf{H} \quad \delta x_p$	$\mathbf{J}_c \quad \delta x_b = \delta x_p$
	$(6{\times}m)(m{\times}1)\ (6{\times}1)$	$(n{\times}6)(6{\times}1)\ (n{\times}1)\ (n{\times}6)(6{\times}1)$	$(6{\times}6)(6{\times}1)\ (6{\times}1)$
	Joints $\quad \rightleftarrows$	**Contact** $\quad \rightleftarrows$	**Object**
Force	$\mathbf{J}_\theta^\top \quad f_f \quad = \tau$	$f_f \quad = \mathbf{H}^\top \ f_{tr} \quad = f_p$	$\mathbf{J}_c^\top \quad f_p \quad = f_b$
	$(m{\times}6)\ (6{\times}1)\ (m{\times}1)$	$(6{\times}1)\ (6{\times}n)\ (n{\times}1)\ (6{\times}1)$	$(6{\times}6)\ (6{\times}1)\ (6{\times}1)$

catenated in an augmented matrix to work in conjunction with the grasp and Jacobian matrices for the analysis of grasping and manipulation.

Table 27.1 summarizes the dual relationship between the force/moment and displacement – a result that is derived from the principle of virtual work. In Table 27.1, $\mathbf{J}_\theta$ is the joint Jacobian matrix relating joint velocities to fingertip velocities, and $\mathbf{J}_c$ is the Cartesian coordinate transformation matrix relating the contact point with the centroidal coordinates of the grasped object. In addition, the number of degrees of freedom (DOFs) in the task space is n and the number of DOFs in the joint spaces is m.

27.4 Rigid–Body Mechanics with Friction

The manipulation planning problem is to choose the motions or forces applied by manipulator contacts so that the part (or parts) moves as desired. This requires solving the subproblem of determining the motion of parts given a particular manipulator action.

Let $q \in \mathbb{R}^n$ be local coordinates describing the combined configuration of the system consisting of one or more parts and robot manipulators, and let $w_i \in \mathbb{R}^6$ represent a wrench at an active contact i, measured in the common coordinate frame O. Let $w_{all} \in \mathbb{R}^{6k}$ be the vector obtained by stacking the w_i, $w_{all} = (w_1^\top \ w_2^\top \ \dots \ w_k^\top)^\top$ (where there are k contacts), and let $\mathbf{A}(q) \in \mathbb{R}^{n \times 6k}$ be a matrix indicating how (or if) each contact wrench acts on each part. (Note that a contact wrench w_i acting on one part means that there is a contact wrench $-w_i$ acting on the other part in contact.) The problem is to find the contact forces w_{all} and the system acceleration $\ddot{q}$, given the state of the system $(q, \dot{q})$, the system mass matrix $M(q)$ and resulting Coriolis matrix $C(q, \dot{q})$, the gravitational forces $g(q)$, the control forces τ, and the matrix $T(q)$ indicating how the control forces τ act on the system. (Alternatively, if we view the manipulators as position controlled, the manipulator components of $\ddot{q}$ can be directly specified and the corresponding components of the control forces τ solved for.) One way to solve this problem is to (a) enumerate the set of all possible contact modes for the current active contacts, and (b) for each contact mode, determine if there are wrenches w_{all} and accelerations $\ddot{q}$ that satisfy the dynamics

$$A(q)w_{all} + T(q)\tau - g(q) = M(q)\ddot{q} + C(q, \dot{q})\dot{q} \tag{27.14}$$

and that are consistent with the contact mode's kinematic constraints (constraints on $\ddot{q}$) and friction cone force constraints (constraints on w_{all}). This formulation is quite general and applies to multiple parts in contact. Equation (27.14) may be simplified by appropriate representations of the configurations and velocities of rigid-body parts (for example, using angular velocities of the rigid bodies instead of derivatives of local angular coordinates).

This formulation leads to some surprising conclusions: there may be multiple solutions to a particular problem (ambiguity) or there may be no solutions (inconsistency) [27.7–14]. This strange behavior arises from the status of Coulomb's law as an approximate law, and it disappears for zero friction, or friction that is small enough. Despite this weakness of the Coulomb friction law, it is a useful approximation. Nonetheless, if we would like to prove (under the Coulomb model) that a particular desired part motion occurs, we generally must also show that no other motion can occur. Other-

wise we have only shown that the desired motion is one of the possible outcomes.

27.4.1 Complementarity

The conditions that each contact provides an equal number of motion constraints and wrench freedoms (Sect. 27.3.2) can be written as *complementarity* conditions. Thus the problem of solving (27.14), subject to contact constraints, can be formulated as a complementarity problem (CP) [27.12, 13, 43–46]. For planar problems, or spatial problems with approximate pyramidal friction cones, the problem is a linear complementarity problem [27.47]. For circular spatial friction cones, the problem is a nonlinear complementarity problem, due to the quadratic constraints describing the cones. In either case, standard algorithms can be used to solve for possible contact modes and part motions.

Alternatively, assuming linearized friction cones, we can formulate a linear constraint satisfaction program (LCSP) for each contact mode (e.g., a linear program with no objective function). The contact mode places linear constraints on the part accelerations, and the solver solves for the part accelerations and the nonnegative coefficients multiplying each of the edges of the friction cones, subject to the dynamics (27.14). Each LCSP with a feasible solution represents a feasible contact mode.

27.4.2 Quasistatic Assumption

A common assumption in robot manipulation planning is the *quasistatic* assumption. This assumption says that parts move slowly enough that inertial effects are negligible. This means that the right- and left-hand sides of (27.14) are zero. With this assumption, we often solve for part *velocities* rather than accelerations. These velocities must be consistent with the kinematic constraints and force constraints, and forces acting on the parts must always sum to zero.

27.4.3 Examples

While rigid-body mechanics problems with friction are usually solved using computational tools for CPs and LCSPs, equivalent graphical methods can be used for some planar problems to assist the intuition. As a simple example, consider the pipe clamp in Fig. 27.6 [27.14]. Under the external wrench $\boldsymbol{w}_{ext}$, does the clamp slide down the pipe, or does it remain fixed in place? The figure uses moment labeling to represent the composite wrench cone of contact forces that can act on the
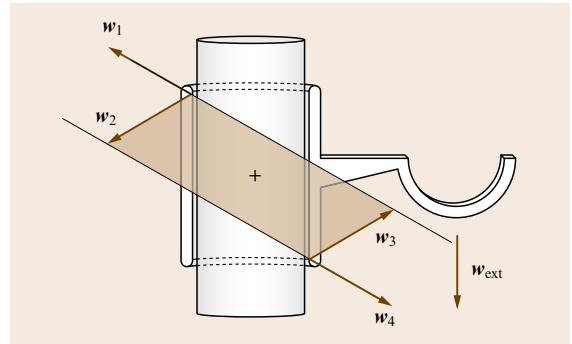

Fig. 27.6 The moment-labeling representation of the composite wrench cone of contact forces the pipe can apply to the pipe clamp. In this figure, the wrench $\boldsymbol{w}_{ext}$ applied to the pipe clamp can be resisted by forces within the composite wrench cone

clamp from the pipe. The wrench $\boldsymbol{w}_{ext}$ acting on the clamp can be exactly balanced by a wrench in the composite wrench cone. This is evident from the fact that the wrench opposing $\boldsymbol{w}_{ext}$ passes around the + labeled region in a counterclockwise sense, meaning that it is contained in the contact wrench cone. As a result, static equilibrium (the ff contact mode) is a feasible solution for the pipe clamp. To arrive at the same result using an LCSP, label the unit wrenches at the edges of the friction cones $\boldsymbol{w}_1, \dots, \boldsymbol{w}_4$. Then the clamp can remain at rest if there exist coefficients $a_1, \dots, a_4$ such that

$$a_1, a_2, a_3, a_4 \geq 0 \,,$$
$$a_1\boldsymbol{w}_1 + a_2\boldsymbol{w}_2 + a_3\boldsymbol{w}_3 + a_4\boldsymbol{w}_4 + \boldsymbol{w}_{ext} = 0 \,.$$

To show that static equilibrium is the only solution, all other contact modes must be ruled out. Note that, if the friction coefficient at the contacts is too small, the clamp will fall under $\boldsymbol{w}_{ext}$.
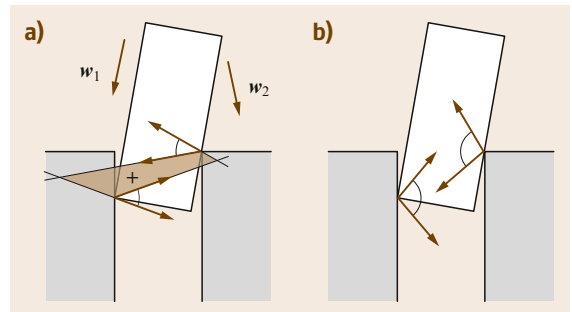
Fig. 27.7 (a) The peg will proceed into the hole under the external wrench $\boldsymbol{w}_1$ but will get stuck under the wrench w_2. **(b)** The peg is wedged
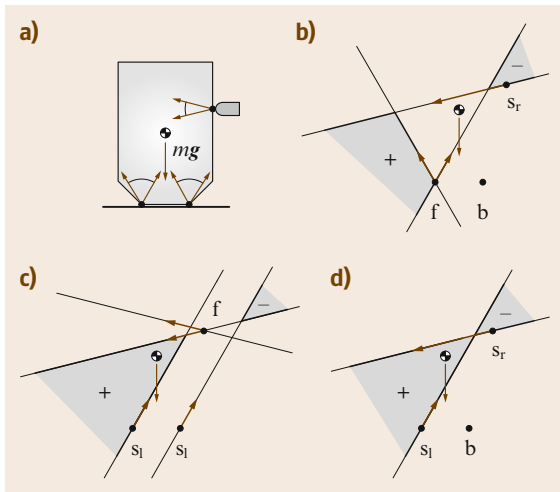
Fig. 27.8 **(a)** A finger moves *left* into a planar block resting on a table in gravity. The contact friction cones are shown. **(b)** Possible contact forces for the contact label f at the leftmost bottom contact, b at the rightmost bottom contact, and r at the pushing contact. This contact mode fbr corresponds to the block tipping over the leftmost contact. Note that the contact wrench cone (represented by moment labels) can provide a force that exactly balances the gravitational force. Thus this contact mode is quasistatically possible. **(c)** The contact wrench cone for the llf contact mode (block slides *left* on the table) cannot balance the gravitational force. This contact mode is not quasistatically possible. **(d)** The contact wrench cone for the lbr contact mode (block slides and tips) is not quasistatically possible

Analysis of the classic peg-in-hole problem is similar to that of the pipe clamp. Figure 27.7a shows an angled peg making two-point contact with the hole. If we apply the wrench $\boldsymbol{w}_1$, the forces from the two-point contact cannot resist, so the ff mode contact mode is not a possibility, and the peg will continue to move into the hole. If we apply the wrench $\boldsymbol{w}_2$, however, the contacts can resist, and the peg will get stuck. This is called *jamming* [27.48]. If there is higher friction at the contacts, as in Fig. 27.7b, then each friction cone may be able to see the base of the other, and the feasible contact wrenches span the entire wrench space [27.49]. In this case, any wrench we apply may be resisted by the contacts. The peg is said to be *wedged* [27.48]. Whether or not the peg will actually resist our applied wrench depends on how much internal force acts between the contacts. This cannot be answered by our rigid-body model; it requires a compliant contact model, as discussed in Sect. 27.6.
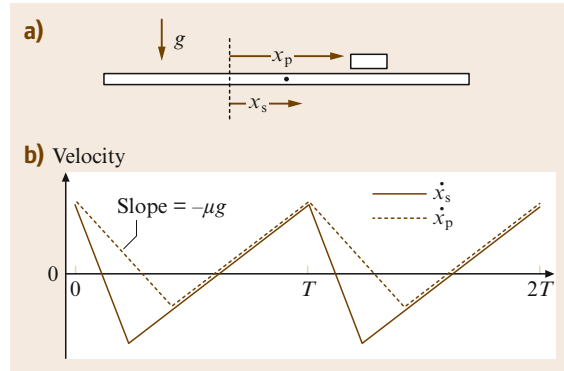
Fig. 27.9 **(a)** A part supported by a horizontally vibrating surface. **(b)** Friction between the part and the surface causes the part to always try to catch up to the surface, but its acceleration is bounded by $\pm\mu g$. The asymmetric motion of the surface gives the part an average positive velocity over a cycle

As a slightly more complex quasistatic example, consider a block on a table being pushed by a finger that moves horizontally to the left (Fig. 27.8) [27.50, 51]. Does the part begin to tip over, slide, or both tip and slide? The corresponding contact modes are $\mathrm{fbs_r}$, $\mathrm{s_ls_lf}$, and $\mathrm{s_lbs_r}$, as shown in Fig. 27.8. The figure also shows the composite contact wrench cones using moment labels. It is clear that quasistatic balance between the gravitational force and the contact wrench cone can only occur for the tipping without slipping contact mode $\mathrm{fbs_r}$. Therefore, the only quasistatic solution is that the block begins to tip without sliding, and the speed of this motion is determined by the speed of the finger's motion. The graphical construction can be used to confirm our intuition that tipping of the block occurs if we push high on the block or if the friction coefficient at the block's support is high. Try it by pushing a can or glass. Quasistatically, the height of the center of mass is immaterial.

A final example is given in Fig. 27.9. A part of mass m and friction coefficient μ is supported by a horizontal surface that moves periodically in the horizontal direction. The periodic motion consists of a large negative acceleration for a short duration and a smaller positive acceleration for a longer duration. The horizontal friction force that can be applied to the part is bounded by $\pm\mu mg$, so the part's horizontal acceleration is bounded by $\pm\mu g$. As a result, the part cannot keep up with the surface as it accelerates backward. Instead, the part slips forward with respect to the surface, which means that the maximal friction force acts in the negative direction, and the part attempts to slow down to the surface's ve-

locity. Eventually the part catches up with the surface as it executes its slow forward acceleration, which is less than μg. Once the part catches up to the surface, it sticks to it, until the next backward acceleration phase. As is evident in Fig. 27.9, the average part velocity over a cycle is positive, so the part moves forward on the surface [27.52, 53]. This idea can be extended to cre-

ate a wide variety of frictional force fields on a rigid plate vibrated with three degrees of freedom in a horizontal plane [27.54, 55] or with a full six degrees of freedom [27.56].

For further examples of manipulation planning using the rigid-body model with Coulomb friction, see [27.14] and the references therein.

27.5 Pushing Manipulation

The friction limit surface (Sect. 27.7) is useful for analyzing pushing manipulation, as it describes the friction forces that can occur as a part slides over a support surface. When the part is pushed with a wrench contained within the limit surface, friction between the part and the support resists the pushing wrench and the part remains motionless. When the part slides quasistatically, the pushing wrench w lies on the limit surface, and the part's twist t is normal to the limit surface at w (Fig. 27.10). When the part translates without rotating, the friction force magnitude is μmg, where m is the part's mass and g is gravitational acceleration. The force applied by the part to the surface is directed through the part's center of mass in the direction of translation.

If the pushing wrench makes positive moment about the part's center of mass, the part will rotate counterclockwise (CCW), and if it makes negative moment
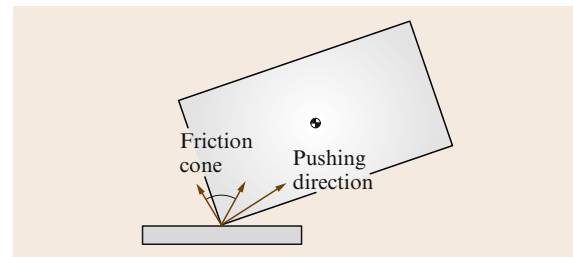
Fig. 27.11 The pusher's motion direction votes for counterclockwise rotation of the part, but it is outvoted by the two edges of the friction cone, which both indicate clockwise rotation
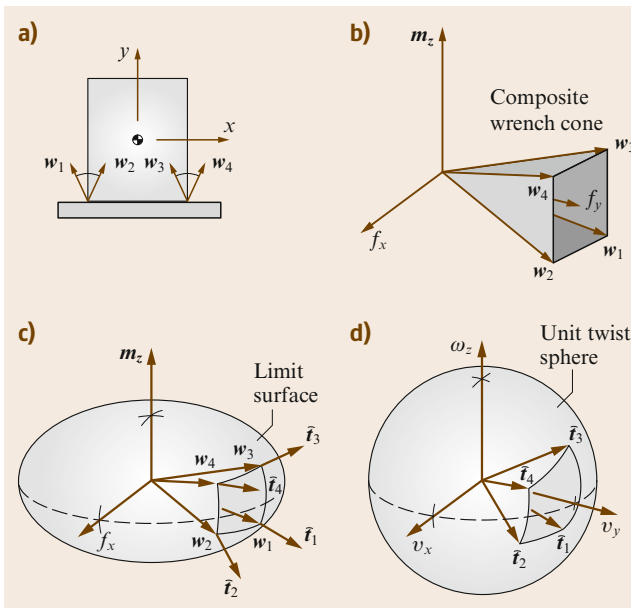
Fig. 27.10 (a) Contact between a pusher and a sliding object. **(b)** The composite contact wrench cone. **(c)** Mapping the wrench cone through the limit surface to twists of the object. **(d)** The unit twists that can result from forces in the composite wrench cone

Fig. 27.12 Stable pushes can be used to maneuver a part among obstacles

about the part's center of mass, it will rotate clockwise (CW). Similarly, if the contact point on the part moves along a line that passes around the part's center of mass in a CW (respectively, CCW) sense, then the part will rotate CW (CCW). From these two observations and considering all possible contact modes, we can conclude that a part pushed at a point contact will rotate CW (CCW) if either (1) both edges of the contact friction cone pass CW (CCW) about the center of mass, or (2) one edge of the friction cone and the pushing direction at the contact both pass around the center of mass in a CW (CCW) sense [27.14, 57], (Fig. 27.11).

This observation allows pushing to be used to reduce uncertainty in part orientation. A series of pushes with a flat fence can be used to completely eliminate the uncertainty in the orientation of a polygonal part [27.57–59]. Bounds on the rate of rotation of parts [27.14, 60, 61] allow the use of a sequence of stationary fences suspended above a conveyor belt to orient parts by pushing them as they are carried along by the conveyor [27.62, 63]. *Stable* pushing plans (Fig. 27.12) use pushing motions that are guaranteed to keep the part fixed to the pusher as it moves, even in the face of uncertainty in the part's pressure distribution [27.14, 64, 65]. Extensions of this work find pushing motions for planar assemblies of parts so that they remain fixed in their relative configurations during motion [27.66–68].

The examples above assume that pushing forces and support friction forces act in the same plane. Other work on pushing has considered three-dimensional effects, where pushing forces are applied above the support plane [27.69].

27.6 Contact Interfaces and Modeling

Contact interface is a general expression to describe the kinematics and kinetics of contacts. Contact applies in various contexts in robotics research; thus, it is more meaningful to refer to generic contact as an *interface*, which is not limited to fingers in grasping and manipulation. The concept of *contact interface* extends the traditional context of physical *contact*. It refers to an interface which imparts kinematic filtering as well as the duality of force/motion transmitted across the contact interface.

Consequently, a contact interface, whether it is rigid or deformable, can be considered as a *kinematic filter* which includes two characteristics: (a) motion and force transmission, and (b) kinematic duality between force/moment and motion. Different contact interfaces will be described in the following sections.

Previous sections of this chapter have assumed rigid bodies in contact. In reality, however, all contacts are accompanied by some deformation of the objects. Often this is by design, as in the case of compliant robot fingertips. When deformation is non-negligible, elastic contact models can be used.

27.6.1 Modeling of Contact Interface

Contact modeling depends on the nature of bodies in contact, including their material properties, applied force, contact deformation, and elastic properties. This section discusses different contact models.

Rigid–Body and Point–Contact Models

With the rigid-body assumption, as discussed in the previous sections of this chapter, two models are often used: (a) *point contact without friction* and (b) *point contact with friction*. In the former case, the contact can only apply force in the direction normal to the contact. In the latter case, a tangential friction force is applied in addition to the normal force. The simplest analytical model for point contact with friction is the Coulomb friction model as presented in (27.9).

Hertzian Contact Model

Elastic contact modeling was first studied and formulated more than a century ago by Hertz in 1882 [27.70] based on contact between two linear elastic materials with a normal force which results in very small contact deformation. This is commonly called the *Hertzian* contact and can be found in most mechanics textbooks, such as [27.71, 72]. Hertz made two important explicit assumptions in order for his contact model to be applicable:

1. objects of linear elastic materials in contact
2. small contact deformation compared to the dimension of object

Hertz also conducted experiments using a spherical glass lens against a planar glass plate to validate the contact theory.

Two relevant results of the Hertzian contact theory applied to robotic contact interfaces are summarized as follows. The first pertains to the radius of the contact area. Hertz [27.70] studied the growth of the contact area as a function of the applied normal force N based on the linear elastic model. Based on ten experimental trials, he concluded that the radius of contact is proportional to the normal force raised to the power of $1/3$, which is consistent with the analytical results he derived based on the linear elastic model. That is, the radius of contact, a, is related to the normal force, N, by

$$a \propto N^{\frac{1}{3}} . \tag{27.15}$$

The second result pertains to the pressure distribution over the assumed symmetric contact area – a second-order pressure distribution of the nature of an ellipse or circle. For a symmetric and circular contact area, the pressure distribution is

$$p(r) = \frac{N}{\pi a^2} \sqrt{1 - \left(\frac{r}{a}\right)^2} , \tag{27.16}$$

where N is the normal force, a is the radius of contact, and r is the distance from the center of contact with $0 \leq r \leq a$.

Soft Contact Model
A typical contact interface between a soft finger and contact surface is illustrated in Fig. 27.13. In typical robotic contact interfaces, the materials of the fingertips are not linear elastic. A model that extends linear to nonlinear elastic contact was presented in [27.38] with a power-law equation which subsumes the Hertzian contact theory,

$$a = c \, N^\gamma , \tag{27.17}$$

where $\gamma = n/(2n+1)$ is the exponent of the normal force, n is the strain-hardening exponent, and c is a constant depending on the size and curvature of the fingertip
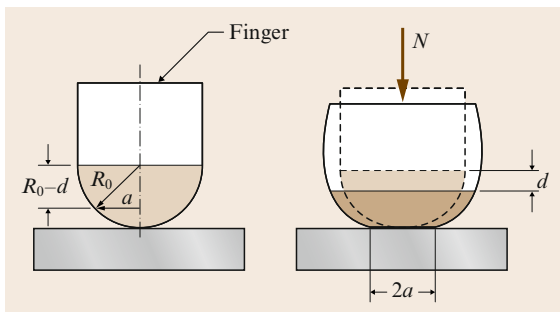
Fig. 27.13 An elastic soft fingertip with a hemispherical tip making contact with a rigid surface

as well as the material properties. Equation (27.17) is the new power law that relates the growth of the circular contact radius to the applied normal force for soft fingers. Note that the equation is derived assuming circular contact area. For linear elastic materials, the constant n is equal to 1 with $\gamma = 1/3$, resulting in the Hertzian contact model in (27.15). Therefore, the soft contact model in (27.17) subsumes the Hertzian contact model.

Other Models
Other models include anthropomorphic contacts and viscoelastic contacts. In modeling viscoelastic contacts, the creep or relaxation phenomenon is incorporated with a time-dependent function, in addition to the elastic deformation described in the general (27.17).

27.6.2 Pressure Distribution at Contacts

In Sect. 27.6.1, when the Hertzian contact theory is considered, the assumed pressure distribution for small elastic deformation is given in (27.16). As the radius of curvature of the two asperities increases and the material properties change to hyperelastic, the pressure distribution becomes more uniform [27.38, 73, 74]. Generalizing equation (27.16), the pressure distribution function for circular contact area with radius a is

$$p(r) = C_k \frac{N}{\pi a^2} \left[1 - \left(\frac{r}{a}\right)^k\right]^{\frac{1}{k}} , \tag{27.18}$$

where N is the normal force, a is the radius of contact, r is the radius with $0 \leq r \leq a$, k determines the shape of the pressure profile, and C_k is a coefficient that adjusts for the profile of pressure distribution over the contact area to satisfy the equilibrium condition. In (27.18), $p(r)$ is defined for $0 \leq r \leq a$. By symmetry, $p(r) = p(-r)$ when $-a \leq r \leq 0$, as shown in Fig. 27.14. When k becomes larger, the pressure distribution approaches uniform distribution, as shown in Fig. 27.14. It is also required that the integral of the pressure over the contact area be equal

Table 27.2 Values of the coefficient C_k in the pressure distribution (27.18),

k	Coefficient C_k
$k = 2$ (circular)	$C_2 = 1.5$
$k = 3$ (cubic)	$C_3 = 1.24$
$k = 4$ (quadruple)	$C_4 = 1.1441$
$k \to \infty$ (uniform)	$C_\infty = 1.0$
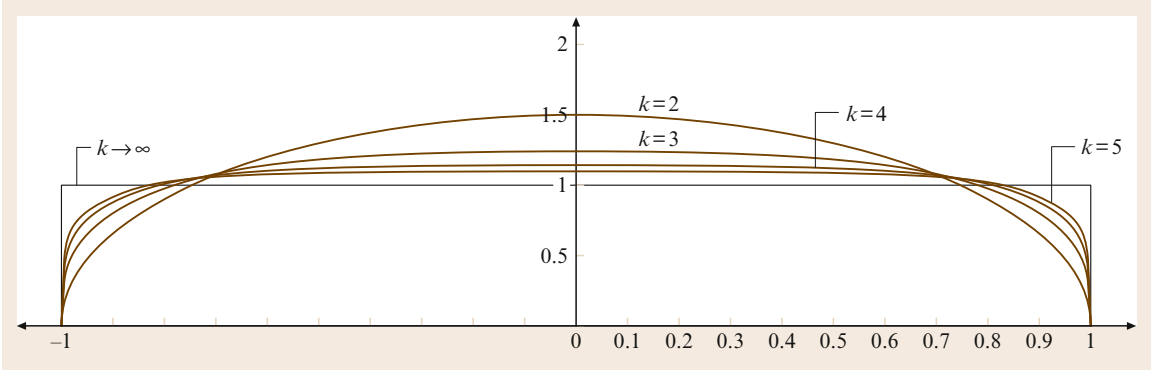
Fig. 27.14 Illustration of pressure distribution with respect to the normalized radius, r/a. The plot shows an axisymmetric pressure distribution with $k = 2, 3, 4, 5$, and ∞. As k increases, the pressure profile becomes more uniform

to the normal force; that is,

$$\int_R p(r)\, \mathrm{d}A = \int_{\theta=0}^{2\pi} \int_{r=0}^{a} p(r)\, r\, \mathrm{d}r\, \mathrm{d}\theta = N\,. \quad (27.19)$$

The coefficient C_k can be obtained by substituting (27.18) into (27.19). It is interesting to note that when (27.19) is integrated, both the normal force and radius of contact vanish, leaving only the constant C_k as follows

$$C_k = \frac{3}{2} \frac{k\Gamma\left(\frac{3}{k}\right)}{\Gamma\left(\frac{1}{k}\right)\Gamma\left(\frac{2}{k}\right)}\,, \quad (27.20)$$

where $k = 1, 2, 3, \cdots$ are typically integer values (although noninteger k values are also possible) and $\Gamma()$ is the gamma function [27.75]. The numerical values of C_k for a few values of k are listed in Table 27.2 for reference. A normalized pressure distribution with respect to the normalized radius, r/a, is plotted in Fig. 27.14. As can be seen from the figure, when k approaches infinity, the pressure profile will become that of a uniformly distributed load with magnitude of $N/(\pi a^2)$, in which case $C_k = 1.0$.

For linear elastic materials, $k = 2$ can be used, although it is found that $k \cong 1.8$ is also appropriate in some cases [27.76]. For nonlinear elastic and viscoelastic materials, the value of k tends to be higher, depending on the properties of the material.

27.7 Friction Limit Surface

Section 27.3 introduced the notion of a wrench cone, describing the set of wrenches that can be applied through a point contact with friction. Any contact wrench is limited to lie within the surface of the cone. This gives rise to the general notion of a *friction limit surface* – the surface bounding the set of wrenches that can be applied through a given contact or set of contacts.

In this section we study the particular case of limit surfaces arising from planar contact patches [27.77, 78]. A planar contact patch occurs when a flat object slides on the floor, a soft robot finger presses against a face of a polyhedron, or a foot of a humanoid robot pushes on the ground. We would like to know what wrenches can be transmitted through such a contact. In the rest of this section, we focus on the properties of the limit sur-

face of a planar contact patch with a specified pressure distribution over the patch.

For ease of discussion, we will call one of the objects in contact the *part* (e.g., the flat object on the floor or the robot finger) and the other object a stationary *support*. We define a coordinate frame so that the planar contact patch is in the $z = 0$ plane, and let $p(r) \geq 0$ be the contact pressure distribution between the part and support as a function of the location $r = (x, y)^\top$. The friction coefficient at the contact patch is μ. If the planar velocity of the part is $t = (\omega_z, v_x, v_y)^\top$, then the linear velocity at r is

$$v(r) = (v_x - \omega_z y, v_y + \omega_z x)^\top\,,$$

and the unit velocity is $\hat{v}(r) = v(r)/\|v(r)\|$. The infinitesimal force applied by the part to the support at r, in the

plane of sliding, is

$$\mathrm{d}\boldsymbol{f}(\boldsymbol{r}) = [\,\mathrm{d}f_x(\boldsymbol{r}),\ \mathrm{d}f_y(\boldsymbol{r})]^\top = \mu\, p(\boldsymbol{r})\hat{\boldsymbol{v}}(\boldsymbol{r})\,. \quad (27.21)$$

The total wrench the part applies to the support is

$$
\begin{aligned}
\boldsymbol{w} &= \begin{pmatrix} m_z \\ f_x \\ f_y \end{pmatrix} \\
&= \int\limits_A \begin{pmatrix} x\,\mathrm{d}f_y(\boldsymbol{r}) - y\,\mathrm{d}f_x(\boldsymbol{r}) \\ \mathrm{d}f_x(\boldsymbol{r}) \\ \mathrm{d}f_y(\boldsymbol{r}) \end{pmatrix} \mathrm{d}A, \quad (27.22)
\end{aligned}
$$

where A is the support area.

As expected, the wrench is independent of the speed of motion: for a given $\boldsymbol{t}_0$ and all $\alpha > 0$, the wrench resulting from velocities $\alpha\boldsymbol{t}_0$ is identical. Viewing (27.22) as a mapping from twists to wrenches, we can map the surface of the unit twist sphere ($\|\hat{\boldsymbol{t}}\| = 1$) to a surface in the wrench space. This surface is the limit surface, and it is closed, convex, and encloses the origin of the wrench space (Fig. 27.15c). The portion of the wrench space enclosed by this surface is exactly the set of wrenches the part can transmit to the support. When the part slips on the support ($\boldsymbol{t} \neq 0$), the contact wrench $\boldsymbol{w}$ lies on the limit surface, and by the maximum-work inequality, the twist $\boldsymbol{t}$ is normal to the limit surface at $\boldsymbol{w}$. If the pressure distribution $p(\boldsymbol{r})$ is finite everywhere, the limit surface is smooth and strictly convex, and the mapping from unit twists to unit wrenches, and vice versa, is continuous and one-to-one. The limit surface also satisfies the property $\boldsymbol{w}(-\hat{\boldsymbol{t}}) = -\boldsymbol{w}(\hat{\boldsymbol{t}})$.
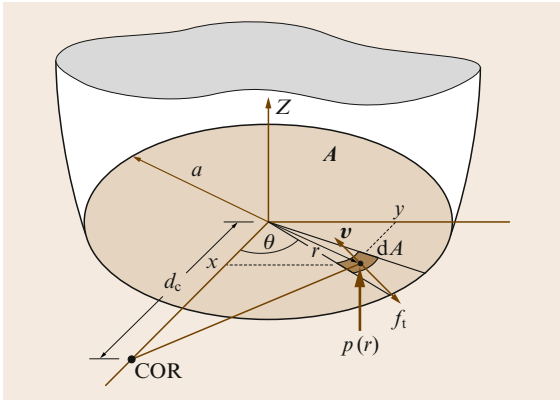
Fig. 27.15 Contact and coordinates for CoR and local infinitesimal area $\mathrm{d}A$ for numerical integration to construct the limit surface of soft fingers

27.7.1 The Friction Limit Surface at a Soft Contact Interface

Given a pressure distribution in (27.18) we can numerically construct the corresponding friction limit surface by using (27.21) and (27.22). For an infinitesimal contact area, the contact resembles a point contact. Hence, the Coulomb's law of friction can be employed.

In the following, we will exploit the kinematic property of center of rotation (CoR) with modeling symmetry to formulate equations for the magnitudes of friction force and moment on a circular contact patch. Figure 27.15 shows a circular contact patch with an instantaneous CoR. By moving (or scanning) the CoR along the x-axis, different possible combinations of friction force and moment can be obtained to construct the limit surface. More details can be found in [27.35–38, 42, 77–80].

The following derivation is for the total friction force (f_t) and moment (m_z) on the contact interface for the CoR at a distance d_c along the x-axis, as shown in Fig. 27.15. By varying the CoR distance d_c from $-\infty$ to ∞, all possible combinations of (f_t, m_z) can be found in order to construct the entire friction limit surface.

The tangential force over the entire contact area can be obtained by integrating shear force on each infinitesimal areas, $\mathrm{d}A$, on which the Coulomb's law of friction is observed, over the entire contact area, A. When Hertzian contact pressure distribution [27.70] is considered, use $k = 2$ in (27.18). Setting $\boldsymbol{r} = (x,\ y)^\top$ and $r = \|\boldsymbol{r}\|$, the total tangential force can be integrated using (27.21) to obtain

$$\boldsymbol{f}_t = \begin{pmatrix} f_x \\ f_y \end{pmatrix} = -\int\limits_A \mu\,\hat{\boldsymbol{v}}(\boldsymbol{r})\,p(r)\,\mathrm{d}A\,, \quad (27.23)$$

where A denotes the circular contact region in Fig. 27.15, $\boldsymbol{f}_t$ is the tangential force vector with the direction shown in Fig. 27.15, μ is the coefficient of friction, $\hat{\boldsymbol{v}}(\boldsymbol{r})$ is the unit vector in the direction of the velocity vector $\boldsymbol{v}(\boldsymbol{r})$ with respect to the CoR on the infinitesimal area $\mathrm{d}A$ at the location $\boldsymbol{r}$, and $p(r)$ is the pressure distribution at distance r from the center of contact. Since the pressure along the annular ring with distance r from the center is the same, we denote it by $p(r)$ instead of $p(\boldsymbol{r})$. The minus sign denotes the opposite directions of $\hat{\boldsymbol{v}}(\boldsymbol{r})$ and $\boldsymbol{f}_t$. Since we are primarily interested in the magnitude of the friction force and moment, we shall omit this sign in the later derivation when magnitudes are concerned.

Similarly, the moment about the z-axis, or the normal to the contact area, is

$$m_z = \int_A \mu \|\boldsymbol{r} \times \hat{\boldsymbol{v}}(\boldsymbol{r})\| \, p(r) \, \mathrm{d}A , \qquad (27.24)$$

where $\|\boldsymbol{r} \times \hat{\boldsymbol{v}}(\boldsymbol{r})\|$ is the magnitude of the cross product of the vectors $\boldsymbol{r}$ and $\hat{\boldsymbol{v}}(\boldsymbol{r})$, whose direction is normal to the contact surface.

The unit vector $\hat{\boldsymbol{v}}(\boldsymbol{r})$ is related to the distance d_c from the origin to the CoR chosen on the x-axis from Fig. 27.15, and can be written as follows

$$\hat{\boldsymbol{v}}(\boldsymbol{r}) = \frac{1}{\sqrt{(x - d_c)^2 + y^2}} \begin{bmatrix} -y \\ (x - d_c) \end{bmatrix}$$
$$= \frac{1}{\sqrt{(r \cos \theta - d_c)^2 + (r \sin \theta)^2}}$$
$$\times \begin{bmatrix} -r \sin \theta \\ (r \cos \theta - d_c) \end{bmatrix} . \qquad (27.25)$$

Due to symmetry, $f_x = 0$ for all CoRs along the x-axis; therefore, the magnitude of the tangential force in the contact tangent plane is $f_t = f_y$. Substituting equations (27.18) and (27.25) into (27.23) and (27.24), we obtain

$$f_t = \int_A \mu \frac{(r \cos \theta - d_c)}{\sqrt{r^2 + d_c^2 - 2 r d_c \cos \theta}} C_k$$
$$\times \frac{N}{\pi a^2} \left[1 - \left(\frac{r}{a} \right)^k \right]^{\frac{1}{k}} \mathrm{d}A . \qquad (27.26)$$

Similarly, the moment about the axis normal to the plane is

$$m_z = \int_A \mu \frac{r^2 - r d_c \cos \theta}{\sqrt{r^2 + d_c^2 - 2 r d_c \cos \theta}} C_k$$
$$\times \frac{N}{\pi a^2} \left[1 - \left(\frac{r}{a} \right)^k \right]^{\frac{1}{k}} \mathrm{d}A . \qquad (27.27)$$

In (27.26) and (27.27), polar coordinates are defined such that $x = r \cos \theta$, $y = r \sin \theta$, and $\mathrm{d}A = r \, \mathrm{d}r \, \mathrm{d}\theta$. We also introduce a normalized coordinate

$$\tilde{r} = \frac{r}{a} . \qquad (27.28)$$

From (27.28), we can write $\mathrm{d}r = a \, \mathrm{d}\tilde{r}$. We also denote $\tilde{d}_c = d_c / a$, and assume that μ is constant throughout the contact area. Substituting the normalized coordinate into equation (27.26) and dividing both sides by μN, we

can derive

$$\frac{f_t}{\mu N} = \frac{C_k}{\pi} \int_0^{2\pi} \int_0^1 \frac{(\tilde{r}^2 \cos \theta - \tilde{r} \tilde{d}_c)}{\sqrt{\tilde{r}^2 + \tilde{d}_c^2 - 2 \tilde{r} \tilde{d}_c \cos \theta}}$$
$$\times (1 - \tilde{r}^k)^{\frac{1}{k}} \, \mathrm{d}\tilde{r} \, \mathrm{d}\theta . \qquad (27.29)$$

Substituting again $\tilde{r} = r/a$ and $\mathrm{d}r = a \, \mathrm{d}\tilde{r}$ into (27.27) and normalizing with $a \mu N$, we obtain

$$\frac{m_z}{a \mu N} = \frac{C_k}{\pi} \int_0^{2\pi} \int_0^1 \frac{(\tilde{r}^3 \cos \theta - \tilde{r}^2 \tilde{d}_c)}{\sqrt{\tilde{r}^2 + \tilde{d}_c^2 - 2 \tilde{r} \tilde{d}_c \cos \theta}}$$
$$\times (1 - \tilde{r}^k)^{\frac{1}{k}} \, \mathrm{d}\tilde{r} \, \mathrm{d}\theta . \qquad (27.30)$$

Equations (27.29) and (27.30) can be numerically integrated for a distance d_c or $\tilde{d}_c$ to yield a point on the limit surface for a prescribed pressure distribution $p(r)$ given by (27.18). Both equations involve elliptic integrals whose closed-form solutions may not exist but can be evaluated numerically. When the CoR distance d_c varies from $-\infty$ to ∞, all possible combinations of (f_t, m_z) can be obtained for plotting the friction limit surface.

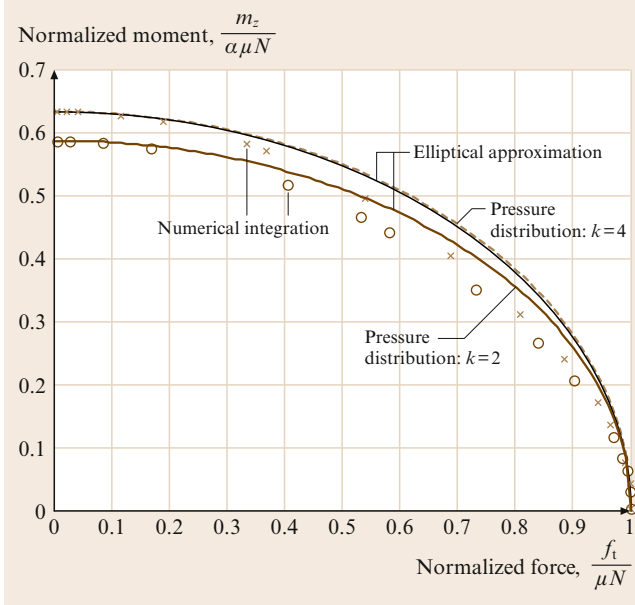### 27.7.2 Example of Constructing a Friction Limit Surface

When the pressure distribution is fourth order with $k = 4$, the coefficient from Table 27.2 is $C_4 = (6/\sqrt{\pi})(\Gamma(3/4)/\Gamma(1/4)) = 1.1441$. Equations (27.29) and (27.30) can be written as

$$\frac{f_t}{\mu N} = 0.3642 \int_0^{2\pi} \int_0^1 \frac{(\tilde{r}^2 \cos \theta - \tilde{r} \tilde{d}_c)}{\sqrt{\tilde{r}^2 + \tilde{d}_c^2 - 2 \tilde{r} \tilde{d}_c \cos \theta}}$$
$$\times (1 - \tilde{r}^4)^{\frac{1}{4}} \, \mathrm{d}\tilde{r} \, \mathrm{d}\theta .$$

$$\frac{m_z}{a \mu N} = 0.3642 \int_0^{2\pi} \int_0^1 \frac{(\tilde{r}^3 \cos \theta - \tilde{r}^2 \tilde{d}_c)}{\sqrt{\tilde{r}^2 + \tilde{d}_c^2 - 2 \tilde{r} \tilde{d}_c \cos \theta}}$$
$$\times (1 - \tilde{r}^4)^{\frac{1}{4}} \, \mathrm{d}\tilde{r} \, \mathrm{d}\theta .$$

Numerical integration for different values of $\tilde{d}_c$ yields pairs of $(f_t/(\mu N), m_z/(a \mu N))$. Plots of these pairs are shown in Fig. 27.16.

A reasonable approximation to these numerical results is given by the following equation of an ellipse

$$\left(\frac{f_t}{\mu N} \right)^2 + \left(\frac{m_z}{(m_z)_{\max}} \right)^2 = 1 , \qquad (27.31)$$

Normalized moment, $\frac{m_z}{\alpha \mu N}$

Normalized force, $\frac{f_t}{\mu N}$

Elliptical approximation

Numerical integration

Pressure distribution: $k = 4$

Pressure distribution: $k = 2$

Fig. 27.16 Example limit surface obtained by numerical integration and elliptical approximation. The numerical integration is based on the pressure distribution, $p(r)$, and the coefficient, C_k. In this figure, the pressure distributions in (27.18) of both $k = 2$ and $k = 4$ are used ◄

a) m_n, f_x, f_y

b) m_n, $(m_n)_{max}$, μN, f_x
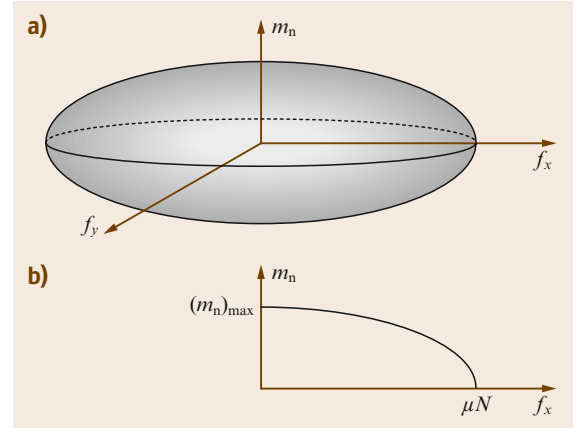
Fig. 27.17a,b Friction limit surface for soft fingers: **(a)** a 3-D ellipsoid representing the limit surface, and **(b)** a section of the ellipsoidal limit surface showing the coupled relationship between the force and moment

where the maximum moment $(m_z)_{max}$ is

$$(m_z)_{max} = \int_A \mu \, |r| C_k \frac{N}{\pi a^2} \left[1 - \left(\frac{r}{a}\right)^k \right]^{\frac{1}{k}} \, dA \, .$$

(27.32)

obtained by (27.27) with the CoR at $d_c = 0$. This defines the quarter-elliptical curves in Fig. 27.16. This approximation is the basis for constructing a three-

dimensional (3-D) ellipsoidal limit surface, as illustrated in Fig. 27.17, and is a good model for the soft contact described in Sect. 27.6.1. More details can be found in [27.35–37, 39, 40, 42, 78].

27.8 Contacts in Grasping and Fixture Designs

It is often important to relate the force and contact displacement (or deformation of contact interface) in grasping and fixture design in which deformable contacts are concerned. Furthermore, such a force–displacement relationship is typically nonlinear due to the nature of contact. A linear expression such as Hooke's law cannot capture the instantaneous and overall characteristics of force and displacement for these contacts. In this section, we formulate and discuss such a relationship using the elastic contact model.

From Fig. 27.13 and the geometry of contact, (27.17), relating the contact radius with normal force, can be rewritten. Assuming $d \ll R_0$, the following equation can be derived [27.39]

$$N = c_d \, d^\zeta \, ,$$

(27.33)

where c_d is a proportional constant, and ζ is

$$\zeta = \frac{1}{2\gamma} \, .$$

(27.34)

Both c_d and ζ can be obtained experimentally. The exponent ζ can also be obtained from γ through (27.34) if γ is already known for the fingertip. The range of the exponent in (27.33) is $\frac{3}{2} \leq \zeta < \infty$. In (27.33), the approach or the vertical depression of the fingertip, d, is proportional to the normal force raised to the power of 2γ (cf. (27.34)) which ranges from 0 to 2/3.

A plot of normal force versus displacement of contact is shown in Fig. 27.18 using (27.33) with a nonlinear power-law equation. Experimental data of contact between a soft finger and flat surface show consistent results when compared with Fig. 27.18 [27.39].
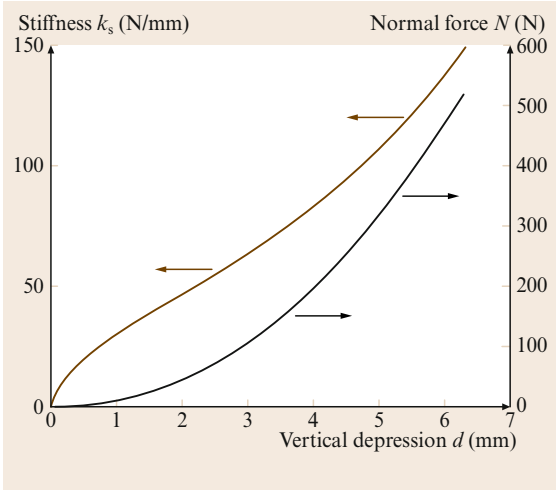
Fig. 27.18 The typical load–depression curve in (27.33) shown with a *scale to the right*, and the contact stiffness, k_s, as given by (27.35) with a *scale to the left*

27.8.1 Contact Stiffness of Soft Fingers

The nonlinear contact stiffness of a soft finger is defined as the ratio of the change in normal force with respect to the change in vertical depression at the contact. The contact stiffness of soft fingers can be obtained by differentiating (27.33) as follows

$$k_s = \frac{\partial N}{\partial d} = c_d \, \zeta \, d^{\zeta-1} = \zeta \left(\frac{N}{d}\right) . \tag{27.35}$$

Substitute (27.33) with $d = \left(\frac{N}{c_d}\right)^{1/\zeta}$ into (27.35) to derive

$$k_s = c_d^{\frac{1}{\zeta}} \, \zeta \, N^{\frac{\zeta-1}{\zeta}} = c_d^{2\gamma} \, \zeta \, N^{1-2\gamma} . \tag{27.36}$$

Thus, the nonlinear contact stiffness of soft fingers, derived in a succinct form in (27.35), is the product of the exponent ζ and the ratio of the normal force versus the approach, N/d. A typical contact stiffness as a function of vertical depression is plotted in Fig. 27.18. The stiffness shown in the figure increases with the force. The expressions for the stiffness, k_s, as a function of various parameter(s) are summarized in the following Table 27.3.

Table 27.3 Summary of equations of contact stiffness

	$f(d)$	$f(N)$	$f(N,d)$
k_s	$c_d \zeta d^{\zeta-1}$	$c_d^{\frac{1}{\zeta}} \zeta N^{\frac{\zeta-1}{\zeta}}$	$\zeta \left(\frac{N}{d}\right)$

The change in stiffness can be obtained by differentiating (27.35) to derive the following equations:

$$\frac{\partial k_s}{\partial d} = c_d \, \zeta(\zeta - 1) \, d^{\zeta-2} , \tag{27.37}$$

$$\frac{\partial k_s}{\partial N} = \frac{\zeta - 1}{d} . \tag{27.38}$$

Equation (27.35) suggests that the stiffness of soft contacts always increases because the ratio N/d always increases, with constant ζ for prescribed fingertip material and range of normal force. This is consistent with the observation that the contact stiffness becomes larger (i. e., stiffer) with larger depression and force. Additionally, (27.38) suggests that the contact stiffness k_s always increases with the normal force because $\partial k_s/\partial N > 0$ owing to $\zeta \geq 1.5$. Moreover, the change in stiffness with respect to the normal load is inversely proportional to the vertical depression, d, as derived in (27.38). This result asserts that the rate of increase in the contact stiffness will gradually become less and less as the normal load and vertical depression increase.

A summary of the equations for soft fingers is presented in Table 27.4. The range of the exponent of the general power-law equation in (27.17) is $0 \leq \gamma \leq 1/3$. The Hertzian contact has an exponent of $\gamma = 1/3$; therefore, the Hertzian contact theory for linear elastic materials is a special case of (27.17). Linear elastic materials, such as steel or other metallic fingertips, under small deformation, generally follow the Hertzian contact theory fairly well. The power-law equation in (27.17) should be employed for fingertips made of softer materials, such as soft rubber or silicone or even viscoelastic fingertips.

27.8.2 Application of Soft Contact Theory to Fixture Design

The preceding analysis and results can be applied in fixturing design and other applications that involve contact with finite areas [27.6]. In fixture design with soft contacts (e.g., copper surfaces) under relatively large deformation and load, the power-law equations in Table 27.4 should be considered in place of the Hertzian contact equation. In these cases, the Hertzian contact model is no longer accurate and should be replaced. On the other hand, if linear elastic materials are used in fixture design with relatively small deformation ($d/R_0 \leq 5\%$), the exponent should be taken as $\gamma = 1/3$ when applying the contact theory. Furthermore, the exponent γ was found to be material dependent and not geometry dependent in general [27.38]. Once the value of γ is determined

Table 27.4 Summary of the contact mechanics equations for linear elastic (when $\gamma = 1/3$ or $\zeta = 3/2$) and nonlinear elastic soft fingers

Description	Equation for soft fingers	Parameters
Power law	$a = c\,N^{\gamma}$	$0 \leq \gamma \leq \frac{1}{3}$
Pressure distribution	$p(r) = p(0)\left[1 - \left(\frac{r}{a}\right)^k\right]^{\frac{1}{k}}$	Typically $k \geq 1.8$
Contact approach	$N = c_{\mathrm{d}}\,d^{\zeta}$	$\frac{3}{2} \leq \zeta \leq \infty$
Contact stiffness	$k_{\mathrm{s}} = \zeta\frac{N}{d}$	Nonlinear

for the material (for example, using a tensile testing machine with the experimental procedure in [27.38]), it can be employed for the analysis of fixturing design using the relevant equations presented herewith.

27.9 Conclusions and Further Reading

In this chapter, both rigid-body and elastic models of contact interfaces are discussed, including kinematic constraints and the duality between the contact wrenches and twists. Contact forces that may arise with Coulomb friction are described. Multiple-contact manipulation tasks with rigid-body and Coulomb friction are presented. The friction limit surface is introduced and utilized to analyze pushing problems. An example of constructing a friction limit surface for soft contact is presented based on the formulation of force/moment of soft contact interface. Applications of these contact models in fixture analysis and design are presented with the modeling of contact interface. Many references in the bibliography section of this chapter provide further reading on this subject.

Manipulation modes include grasping, pushing, rolling, batting, throwing, catching, casting, and other kinds of quasistatic and dynamic manipulation [27.81].

This chapter presents an overview of contact modeling interfaces, with a particular focus on their use in manipulation tasks, including graspless or *nonprehensile* manipulation modes such as pushing. Analyses of grasps and fixtures are also presented. *Mason*'s textbook [27.14] expands on a number of themes in this chapter, including the theory of polyhedral convex cones, graphical methods for planar problems, and applications to manipulation planning. Fundamental material on polyhedral cones can be found in [27.82] and their application to representations of twists and wrenches in [27.10, 83–85]. Twists and wrenches are elements of classical *screw theory*, which is covered in the texts [27.86, 87] and from the point of view of robotics in the texts [27.30, 88, 89].

In addition, several relevant chapters in this handbook provide further reading for theory and applications, for example, Chaps. 1 and 28.

References

27.1 A. Bicchi: On the problem of decomposing grasp and manipulation forces in multiple whole-limb manipulation, Int. J. Robot. Auton. Syst. **13**, 127–147 (1994)

27.2 K. Harada, M. Kaneko, T. Tsuji: Rolling Based Manipulation for Multiple Objects, Proceedings of IEEE Int. Conf. on Robotics and Automation (San Francisco 2000) pp. 3888–3895

27.3 M.R. Cutkosky, I. Kao: Computing and Controlling The Compliance of a Robotic Hand, IEEE Trans. Robot. Autom., **5**(2), 151–165 (1989)

27.4 M.R. Cutkosky, S.-H. Lee: Fixture Planning with Friction for Concurrent Product/Process Design, NSF Process Planning (1989)

27.5 S.-H. Lee, M. Cutkosky: Fixture planning with friction, ASME J. Eng. Ind. **113**(3), 320–327 (1991)

27.6 Q. Lin, J.W. Burdick, E. Rimon: A stiffness-based quality measure for compliant grasps and fixtures, IEEE Trans. Robot. Autom. **16**(6), 675–688 (2000), ,

27.7 P. Lötstedt: Coulomb friction in two-dimensional rigid body systems, Z. Angew. Math. Mech. **61**, 605–615 (1981)

27.8 P. Lötstedt: Mechanical systems of rigid bodies subject to unilateral constraints, SIAM J. Appl. Math. **42**(2), 281–296 (1982)

27.9 P.E. Dupont: The effect of Coulomb friction on the existence and uniqueness of the forward dynamics problem, International Conference on Robotics and Automation (Nice 1992) pp. 1442–1447

27.10 M.A. Erdmann: On a representation of friction in configuration space, Int. J. Robot. Res. **13**(3), 240–271 (1994)

27.11 K.M. Lynch, M.T. Mason: Pulling by pushing, slip with infinite friction, and perfectly rough surfaces, Int. J. Robot. Res. **14**(2), 174–183 (1995)

27.12 J.S. Pang, J.C. Trinkle: Complementarity formulations and existence of solutions of dynamic multi-rigid-body contact problems with Coulomb friction, Math. Prog. **73**, 199–226 (1996)

27.13 J.C. Trinkle, J.S. Pang, S. Sudarsky, G. Lo: On dynamic multi-rigid-body contact problems with Coulomb friction, Z. Angew. Math. Mech. **77**(4), 267–279 (1997)

27.14 M.T. Mason: *Mechanics of Robotic Manipulation* (MIT Press, Cambrige 2001)

27.15 Y.-T. Wang, V. Kumar, J. Abel: Dynamics of Rigid Bodies Undergoing Multiple Frictional Contacts, Proceedings of IEEE Int. Conf. on Robotics and Automation (Nice, France 1992) pp. 2764–2769

27.16 T.H. Speeter: Three-dimensional finite element analysis of elastic continua for tactile sensing, Int. J. Robot. Res. **11**(1), 1–19 (1992)

27.17 K. Dandekar, A.K. Srinivasan: A 3-Dimensional Finite Element Model of the Monkey Fingertip for Predicting Responses of Slowly Adapting Mechanoreceptors, ASME Bioengineering Conference, Vol. 29 (1995) pp. 257–258

27.18 N. Xydas, M. Bhagavat, I. Kao: Study of Soft-Finger Contact Mechanics Using Finite Element Analysis and Experiments, Proc. IEEE Int. Conf. on Robotics and Automation, ICRA (San Francisco, California 2000)

27.19 K. Komvopoulos, D.-H. Choi: Elastic finite element analysis of multi-asperity contacts, J. Tribol. **114**, 823–831 (1992)

27.20 L.T. Tenek, J. Argyris: *Finite Element Analysis for Composite Structures* (Kluwer Academic, Bosten 1998)

27.21 Y. Nakamura: Contact Stability Measure and Optimal Finger Force Control of Multi-Fingered Robot Hands, Crossing Bridges: Advances in Flexible Automation and Robotics – The Proceedings of the USA-Japan Symposium on Flexible Automation (ASME, 1988) pp. 523–528

27.22 Y.C. Park, G.P. Starr: Optimal Grasping Using a Multifingered Robot Hand, Proceedings of the 1990 IEEE International Conference on Robotics and Automation (IEEE, Cincinnati, Ohio 1990) pp. 689–694

27.23 E. Rimon, J. Burdick: On force and form closure for multiple finger grasps, IEEE International Conference on Robotics and Automation (1996) pp. 1795–1800

27.24 E. Rimon, J.W. Burdick: New bounds on the number of frictionless fingers required to immobilize planar objects, J. Robot. Sys. **12**(6), 433–451 (1995)

27.25 E. Rimon, J.W. Burdick: Mobility of bodies in contact–part I: A 2nd-order mobility index for multiple-finger grasps, IEEE Trans. Robot. Autom. **14**(5), 696–708 (1998)

27.26 D.J. Montana: The kinematics of contact and grasp, Int. J. Robot. Res. **7**(3), 17–32 (1988)

27.27 C.S. Cai, B. Roth: On the planar motion of rigid bodies with point contact, Mechanism Machine Theory **21**(6), 453–466 (1986)

27.28 C. Cai, B. Roth: On the spatial motion of a rigid body with point contact, IEEE International Conference on Robotics and Automation (1987) pp. 686–695

27.29 A.B.A. Cole, J.E. Hauser, S.S. Sastry: Kinematics and control of multifingered hands with rolling contact, IEEE Trans. Autom. Control **34**(4), 398–404 (1989)

27.30 R.M. Murray, Z. Li, S.S. Sastry: *A Mathematical Introduction to Robotic Manipulation* (CRC, Boca Raton 1994)

27.31 F. Reuleaux: *The Kinematics of Machinery* (Dover, New York 1963), , reprint of MacMillan, 1876

27.32 C.A. Coulomb: Theorie des machines simples en ayant egard au frottement de leurs parties et a la roideur des cordages. In: *Memoires des mathematique et de physique presentes a l'Academie des Sciences* (Bachelier, Paris 1821)

27.33 Y. Maeda, T. Arai: Planning of graspless manipulation by a multifingered robot hand, Adv. Robot. **19**(5), 501–521 (2005)

27.34 M.T. Mason: Two graphical methods for planar contact problems, IEEE/RSJ International Conference on Intelligent Robots and Systems (Osaka, Japan November 1991) pp. 443–448

27.35 R. Howe, I. Kao, M. Cutkosky: Sliding of Robot Fingers Under Combined Torsion and Shear Loading, Proceedings of 1988 IEEE International Conference on Robotics and Automation, Vol. 1 (Philadelphia, Pennsylvania 1988) pp. 103–105

27.36 I. Kao, M.R. Cutkosky: Dextrous manipulation with compliance and sliding, Int. J. Robot. Res. **11**(1), 20–40 (1992)

27.37 R.D. Howe, M.R. Cutkosky: Practical force-motion models for sliding manipulation, Int. J. Robot. Res. **15**(6), 555–572 (1996)

27.38 N. Xydas, I. Kao: Modeling of contact mechanics and friction limit surface for soft fingers with experimental results, Int. J. Robot. Res. **18**(9), 941–950 (1999)

27.39 I. Kao, F. Yang: Stiffness and contact mechanics for soft fingers in grasping and manipulation, IEEE Trans. Robot. Autom. **20**(1), 132–135 (2004), ,

27.40 J. Jameson, L. Leifer: Quasi-Static Analysis: A Method for Predicting Grasp Stability, Proceedings

of 1986 IEEE International Conference on Robotics and Automation (1986) pp. 876–883

27.41 S. Goyal, A. Ruina, J. Papadopoulos: Planar sliding with dry friction: Part 2. Dynamics of motion, Wear **143**, 331–352 (1991)

27.42 P. Tiezzi, I. Kao: Modeling of viscoelastic contacts and evolution of limit surface for robotic contact interface, IEEE Trans. Robot. **23**(2), 206–217 (2007)

27.43 M. Anitescu, F. Potra: Formulating multi-rigid-body contact problems with friction as solvable linear complementarity problems, ASME J. Nonlin. Dyn. **14**, 231–247 (1997)

27.44 S. Berard, J. Trinkle, B. Nguyen, B. Roghani, J. Fink, V. Kumar: daVinci code: A multi-model simulation and analysis tool for multi-body systems, IEEE International Conference on Robotics and Automation (2007)

27.45 P. Song, J.-S. Pang, V. Kumar: A semi-implicit time-stepping model for frictional compliant contact problems, Int. J. Numer. Methods Eng. **60**(13), 2231–2261 (2004)

27.46 D. Stewart, J. Trinkle: An implicit time-stepping scheme for rigid body dynamics with inelastic collisions and Coulomb friction, Int. J. Numer. Methods Eng. **39**, 2673–2691 (1996)

27.47 R.W. Cottle, J.-S. Pang, R.E. Stone: *The Linear Complementarity Problem* (Academic, New York 1992)

27.48 S.N. Simunovic: Force information in assembly processes, International Symposium on Industrial Robots (1975)

27.49 V.-D. Nguyen: Constructing force-closure grasps, Int. J. Robot. Res. **7**(3), 3–16 (1988), ,

27.50 K.M. Lynch: Toppling manipulation, IEEE International Conference on Robotics and Automation (1999)

27.51 M.T. Zhang, K. Goldberg, G. Smith, R.-P. Berretty, M. Overmars: Pin design for part feeding, Robotica **19**(6), 695–702 (2001)

27.52 D. Reznik, J. Canny: The Coulomb pump: a novel parts feeding method using a horizontally-vibrating surface, IEEE International Conference on Robotics and Automation (1998) pp. 869–874

27.53 A.E. Quaid: A miniature mobile parts feeder: Operating principles and simulation results, IEEE International Conference on Robotics and Automation (1999) pp. 2221–2226

27.54 D. Reznik, J. Canny: A flat rigid plate is a universal planar manipulator, IEEE International Conference on Robotics and Automation (1998) pp. 1471–1477

27.55 D. Reznik, J. Canny: C'mon part, do the local motion!, IEEE International Conference on Robotics and Automation (2001) pp. 2235–2242

27.56 T. Vose, P. Umbanhowar, K.M. Lynch: Vibration-induced frictional force fields on a rigid plate, IEEE International Conference on Robotics and Automation (2007)

27.57 M.T. Mason: Mechanics and planning of manipulator pushing operations, Int. J. Robot. Res. **5**(3), 53–71 (1986)

27.58 K.Y. Goldberg: Orienting polygonal parts without sensors, Algorithmica **10**, 201–225 (1993)

27.59 R.C. Brost: Automatic grasp planning in the presence of uncertainty, Int. J. Robot. Res. **7**(1), 3–17 (1988)

27.60 J.C. Alexander, J.H. Maddocks: Bounds on the friction-dominated motion of a pushed object, Int. J. Robot. Res. **12**(3), 231–248 (1993)

27.61 M.A. Peshkin, A.C. Sanderson: The motion of a pushed, sliding workpiece, IEEE J. Robot. Autom. **4**(6), 569–598 (1988)

27.62 M.A. Peshkin, A.C. Sanderson: Planning robotic manipulation strategies for workpieces that slide, IEEE J. Robot. Autom. **4**(5), 524–531 (1988)

27.63 M. Brokowski, M. Peshkin, K. Goldberg: Curved fences for part alignment, IEEE International Conference on Robotics and Automation (Atlanta 1993) pp. 467–473

27.64 K.M. Lynch: The mechanics of fine manipulation by pushing, IEEE International Conference on Robotics and Automation (Nice 1992) pp. 2269–2276

27.65 K.M. Lynch, M.T. Mason: Stable pushing: Mechanics, controllability, and planning, Int. J. Robot. Res. **15**(6), 533–556 (1996)

27.66 K. Harada, J. Nishiyama, Y. Murakami, M. Kaneko: Pushing multiple objects using equivalent friction center, IEEE International Conference on Robotics and Automation (2002) pp. 2485–2491

27.67 J.D. Bernheisel, K.M. Lynch: Stable transport of assemblies: Pushing stacked parts, IEEE Trans. Autom. Sci. Eng. **1**(2), 163–168 (2004)

27.68 J.D. Bernheisel, K.M. Lynch: Stable transport of assemblies by pushing, IEEE Trans. Robot. **22**(4), 740–750 (2006)

27.69 H. Mayeda, Y. Wakatsuki: Strategies for pushing a 3D block along a wall, IEEE/RSJ International Conference on Intelligent Robots and Systems (Osaka, Japan 1991) pp. 461–466

27.70 H. Hertz: On the Contact of Rigid Elastic Solids and on Hardness. In: *6: Assorted Papers by H. Hertz*, ed. by H. Hertz (MacMillan, New York 1882)

27.71 K.L. Johnson: *Contact Mechanics* (Cambridge Univ. Press, Cambridge 1985)

27.72 S.P. Timoshenko, J.N. Goodier: *Theory of Elasticity*, 3rd edn. (McGraw-Hill, New York 1970)

27.73 E. Wolf: *Progress in Optics* (North-Holland, Amsterdam 1992)

27.74 E.J. Nicolson, R.S. Fearing: The Reliability of Curvature Estimates from Linear Elastic Tactile Sensors, the Proceedings of the 1995 IEEE International Conference on Robotics and Automation (IEEE Press 1995)

27.75 M. Abramowitz, I. Stegun: *Handbook of Mathematical Functions with formulas, graphs, and*

mathematical tables, 7th edn. (Dover, New York 1972)

27.76 I. Kao, S.-F. Chen, Y. Li, G. Wang: Application of bio-engineering contact interface and MEMS in robotic and human augmented systems, IEEE Robot. Autom. Mag. **10**(1), 47–53 (2003)

27.77 S. Goyal, A. Ruina, J. Papadopoulos: Planar sliding with dry friction. Part 1. Limit surface and moment function, Wear **143**, 307–330 (1991)

27.78 S. Goyal, A. Ruina, J. Papadopoulos: Planar sliding with dry friction. Part 2. Dynamics of motion, Wear **143**, 331–352 (1991)

27.79 J.W. Jameson: Analytic Techniques for Automated Grasp. Ph.D. Thesis (Department of Mechanical Engineering, Stanford University 1985)

27.80 S. Goyal, A. Ruina, J. Papadopoulos: Limit Surface and Moment Function Description of Planar Sliding, Proceedings of 1989 IEEE International Conference on Robotics and Automation (IEEE Computer Society, Scottsdale, Arizona 1989) pp.794–799

27.81 K.M. Lynch, M.T. Mason: Dynamic nonprehensile manipulation: Controllability, planning, and experiments, Int. J. Robot. Res. **18**(1), 64–92 (1999)

27.82 A.J. Goldman, A.W. Tucker: Polyhedral convex cones. In: *Linear Inequalities and Related Systems*, ed. by H.W. Kuhn, A.W. Tucker (Princeton Univ. Press, Princeton 1956)

27.83 M.A. Erdman: A configuration space friction cone;, IEEE/RSJ International Conference on Intelligent Robots and Systems (Osaka, 1991) pp.455–460

27.84 M.A. Erdmann: Multiple-point contact with friction: Computing forces and motions in configuration space, IEEE/RSJ International Conference on Intelligent Robots and Systems (Yokohama, 1993) pp.163–170

27.85 S. Hirai, H. Asada: Kinematics and statics of manipulation using the theory of polyhedral convex cones, Int. J. Robot. Res. **12**(5), 434–447 (1993)

27.86 R.S. Ball: *The Theory of Screws* (Cambridge Univ. Press, Cambridge 1900)

27.87 K.H. Hunt: *Kinematic Geometry of Mechanisms* (Oxford Univ., Oxford 1978)

27.88 J.K. Davidson, K.H. Hunt: *Robots and Screw Theory* (Oxford Univ. Press, Oxfort 2004)

27.89 J.M. Selig: *Geometric Fundamentals of Robotics*, 2nd edn. (Springer, Berlin Heidelberg 2005)

Part D | 27